Application of autoregressive models for optical turbulence prediction at optical communication sites

Florian Quatresooz[a], Ryan Griffiths[b,c], James Osborn[b], Danielle Vanhoenacker-Janvier[a], and Claude Oestges[a]

[a]ICTEAM, Université catholique de Louvain (UCLouvain), Louvain-la-Neuve, Belgium
[b]Centre for Advanced Instrumentation, Durham University, Durham, United Kingdom
[c]Department of Physics, University of Oxford, Oxford, United Kingdom

ABSTRACT

Modelling and forecasting the effects of atmospheric turbulence on the propagation of optical waves is crucial for the development of future free-space optical communication systems. This work explores the use of autoregressive models to provide short-term predictions (i.e., minutes to hours) of optical turbulence integrated parameters, such as the Fried parameter, isoplanatic angle and scintillation index. It exploits measurements from a Shack-Hartmann Image Motion Monitor (SHIMM) instrument at Paranal Observatory, as well as recent data collected in Barcelona during the TURBulence mOnitoring (TURBO) campaign. The study demonstrates that combining long-term forecasts from numerical weather prediction models with on-site measurements using autoregressive models significantly improve short-term predictions. Additionally, autoregressive models based solely on measurements also show good prediction performance. This work motivates future measurement campaigns at optical communication sites to enhance site characterization and optical turbulence modelling, while enabling more accurate short-term forecasts.

Keywords: Optical communication, optical turbulence, numerical weather prediction, autoregressive models

1. INTRODUCTION

Atmospheric turbulence is a major challenge for free-space optical communications between satellites and the Earth's surface. It introduces wavefront distortion and scintillation to the received optical signals, known as optical turbulence (OT). Despite extensive research on this topic for astronomical sites, much work remains to be done in the context of optical communications.[1]

With the recent deployment of optical ground stations (OGS) and the development of compact monitoring instruments,[2,3] various measurement campaigns are underway at potential OGS sites.[4,5] As preliminary data become available, collaborative efforts are focused on refining OT models for optical communication applications.

Modelling and forecasting OT are critical for astronomy, enabling site characterization and flexible scheduling of astronomical observations.[6] Similarly, they play a key role in the characterization of optical communication sites and for the scheduling of optical communication links. Long-term OT forecasts, ranging from hours to days, are typically achieved using numerical weather prediction (NWP) models (i.e., weather forecast models), which are extended to include OT parameters.[6–8] However, with the increasing availability of data, there is a growing interest in short-term forecasts, spanning minutes to hours, that incorporate recent measurements into the predictions. These short-term forecasts are often accomplished using autoregressive (AR) models or machine learning-based approaches.[9,10]

This study explores the use of AR models based on direct measurements, as well as AR models that combine NWP outputs with past measurements. These models are applied to OT integrated parameters (Fried parameter, isoplanatic angle, and scintillation index) collected by a Shack-Hartmann Image Motion Monitor[11] (SHIMM) instrument at Paranal Observatory[2] and in Barcelona.[4] The measurements, taken continuously during daytime and nighttime, enable to characterize OT at both locations. Moreover, the analysis conducted in this work provides valuable insights for designing AR models for short-term forecasting of OT integrated parameters at both astronomical and OGS sites.

Section 2 briefly presents the state-of-the-art in OT short-term forecasting approaches, while Section 3 describes the AR models used and the available measurements. The design of AR models is studied in Section 4 using SHIMM measurements at Paranal, and the models' performance is evaluated and discussed in Sections 5 and 6.

2. SHORT-TERM FORECAST OF OPTICAL TURBULENCE

The application of autoregressive models for seeing prediction was proposed in 1994 during the construction of the Very Large Telescope (VLT) at Paranal, Chile.[12] Since then, AR models have been increasingly applied to OT measurements at various astronomical[13,14] and optical communication sites.[15,16]

Rather than applying AR models directly to the OT time series, they can be used in conjunction with long-term forecasts from NWP models to correct potential biases.[9,17,18] In this approach, AR models are applied to the modelling error, defined as the difference between long-term forecasts and past observations. This method has been successfully implemented for predicting meteorological parameters and seeing conditions at the Large Binocular Telescope[9] and has been extended to other OT quantities at the VLT.[18] It led to significant improvements in the short-term prediction capabilities of the NWP models.

Additionally, recent studies have demonstrated the potential of machine learning (ML) models for short-term OT forecasting.[19] These models often incorporate external inputs, such as meteorological data, to enhance the prediction of OT quantities.[10,14] Another possible approach is the use of regression models that rely on forecast meteorological quantities to then predict OT parameters.[20,21]

This work further explores the application of AR models at astronomical and optical communication sites, in combination with NWP long-term forecasts. The considered AR models are described in the next section.

3. AUTOREGRESSIVE MODELS AND AVAILABLE MEASUREMENTS

Autoregressive models provide a linear framework for describing the temporal evolution of a process, assuming that future values exclusively depend on a linear combination of previous values and on a stochastic term (e.g., noise or model imperfection).[22] The different models used in this work are described below, for a generic scalar quantity y representing any of the OT integrated parameter. This quantity is measured at discrete time instants t_k, yielding a series of measurements $y_k = y(t_k)$, where $k \in \mathbb{N}$ denotes the temporal index of the series. The use of AR models enables to predict the value of y_k, denoted $\hat{y}_k$, based on the observed time series $y_{0:k-1}$ for all previous time instants (one-step ahead predictions). Multistep ahead predictions are also possible, i.e., estimating y_{k+n} knowing $y_{0:k-1}$ ($n+1$-step ahead predictions), for $n \in \mathbb{N}$.

Persistence model This simple model is used as a benchmark for the evaluation of the other models. Its prediction of the next value in the time series is equal to its most recent measurement, i.e.,

$$\hat{y}_k = y_{k-1}. \tag{1}$$

For multistep ahead predictions, the last available observation is used, i.e., $\hat{y}_{k+n} = y_{k-1}$.

Autoregression on measurements In this model, the predicted $\hat{y}_k$ comes from a linear combination of previous measurements, weighted by coefficients α_i. The time horizon of this combination is set to N, i.e.,

$$\hat{y}_k = \alpha_0 + \sum_{i=1}^{N} \alpha_i \; y_{k-i}. \tag{2}$$

The coefficients α_i for $i \in \{0, \ldots, N\}$ must be determined and "learned" based on a set of measurements. The coefficient α_0 is a constant in the AR model. Equation (2) behaves as a sliding window of width N on the time series, in which measured values of y are weighted and summed to give $\hat{y}_k$. Multistep predictions are made recursively, using

$$\hat{y}_{k+n} = \alpha_0 + \sum_{i=1}^{n} \alpha_i \ \hat{y}_{k+n-i} + \sum_{i=1}^{N-n} \alpha_{i+n} \ y_{k-i} \tag{3}$$

for a $n+1$-step prediction, knowing $y_{0:k-1}$. It shows that the available observations in $y_{0:k-1}$ appear weighted by corresponding AR coefficients, while the other variables $y_{k:k+n-1}$ are substituted by their estimations since they have not been observed yet.

Autoregression on the modelling error In scenarios where a forecast sequence $y^{(\text{mod.})}$ from another model is available, such as from NWP models, the autoregression can be performed on the modelling error,[9,18] defined by $x_k = y_k - y_k^{(\text{mod.})}$. The one-step ahead predicted value $\hat{y}_k$ from the autoregression is given by

$$\hat{y}_k = y_k^{(\text{mod.})} + x_k \ \text{ with } \ x_k = \alpha_0 + \sum_{i=1}^{N} \alpha_i \ \underbrace{\left(y_{k-i} - y_{k-i}^{(\text{mod.})}\right)}_{=x_{k-i}}, \tag{4}$$

where the coefficients α_i for $i \in \{0, \ldots, N\}$ must also be determined from a set of available measurements. Multistep ahead predictions are performed using a similar expression as (3).

In this study, the AR model coefficients are estimated using the statsmodels Python package.[23]

Available measurements and illustration Short-term forecasts using AR models are applied to measurements of OT integrated parameters collected by the SHIMM (24hSHIMM) instrument[11] at Paranal Observatory (24.62615°S, 70.40387°W, altitude 2625 m), Chile, and at Universitat Politècnica de Catalunya (41.38922°N, 2.11205°E, altitude 115 m), Barcelona, Spain.

The Paranal campaign consists of six days of nearly continuous measurements, from February 28th to March 5th, 2023.[2] Results of the campaign have been previously used to validate Fried parameter r_0 predictions from NWP models[8] and are extended here to the isoplanatic angle θ_0 and the scintillation index σ_I^2. The measured time series by the SHIMM instrument and the predicted time series using NWP models are given in Figure 6 in Appendix A. Measurements (blue dots) have been averaged over 5-minute bins, and their uncertainty is depicted by the vertical bars. Plain lines are associated to two different parametrizations of the NWP models, one relying on the turbulent kinetic energy (TKE) and another based on the Tatarskii equation with a boundary layer (BL) extension using Monin-Obukhov similarity theory.[8,24] The NWP software used is the Weather Research and Forecasting (WRF) software.[25]

OT measurement in Barcelona have been acquired during the TURBulence mOnitoring (TURBO) campaign, in November 2023 and May 2024.[4] The time series are given in Figures 7 and 8 of Appendix A, corresponding respectively to two and three days of nearly continuous data. The modelled time series come from the same NWP models as for the observations at Paranal. Significant discrepancies are observed between the measured and modelled isoplanatic angles, for both NWP models. The TKE model performs better for modelling the Fried parameter during the day, while the Tatarskii+BL model is more effective at night.

As an example, Figure 1 illustrates the application of the three models in (1) to (4) for short-term forecasting of the Fried parameter at Paranal. The autoregressive models on measurements and modelling errors (each with ten coefficients, $N = 10$) were fitted using a four-hour window of data (8:00 to 12:00 UTC on March 4) and used to predict the next hour using multistep ahead predictions. Only the TKE model is considered for obtaining $y^{(\text{mod.})}$. The persistence model, as expected, provides a constant forecast based on the last measurement, while the AR models predict a slight decrease in the Fried parameter. The actual measurements during the prediction period (depicted by light blue squares) indicate that the AR models offer more accurate predictions compared to the persistence model in this studied case.

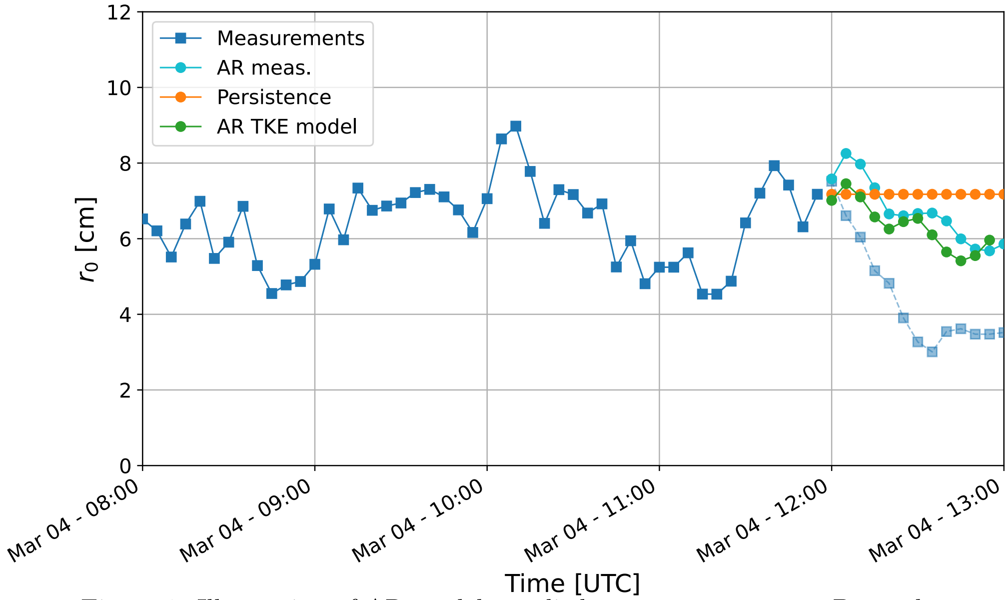

Figure 1: Illustration of AR models applied to measurements at Paranal.

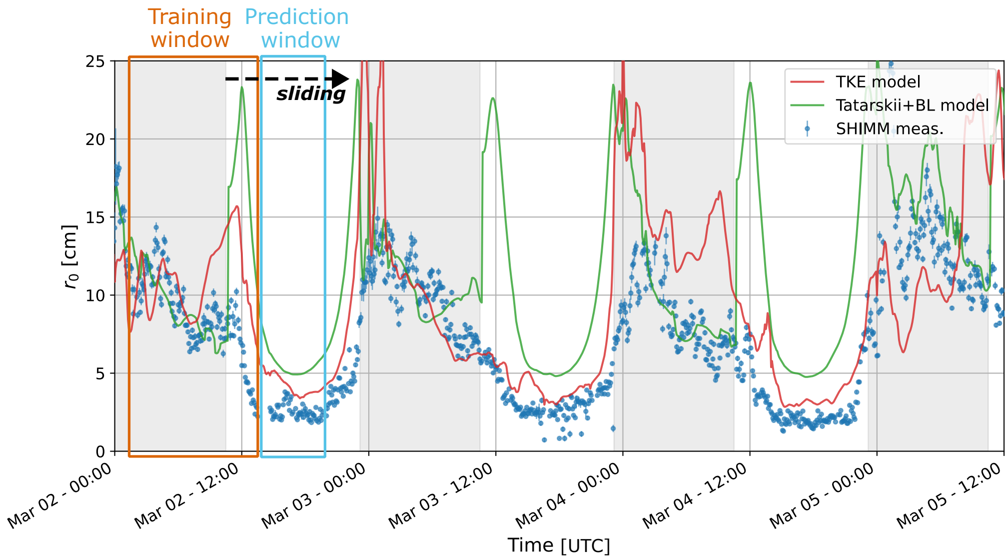

Figure 2: Data used for designing the AR models, and definitions of training and prediction windows.

4. DESIGN OF AUTOREGRESSIVE MODELS

The application to practical scenarios of the AR models given in (2) and (4) requires the determination of the number of coefficients N in the autoregression, the training window duration (used to fit the AR coefficients), and the prediction window duration (i.e., the time horizon for the forecast). These parameters are analysed using data collected at Paranal during the last three days and four nights of continuous measurements, as illustrated in Figure 2 for the Fried parameter. The training and prediction windows, defined in the figure, are progressively shifted with a 5-minute time step to evaluate the performance metrics, by comparing forecasts to measurements within the prediction window. In cases of isolated missing data, gaps in the time series are filled with the previous measured values, which may artificially increase the performance of the persistence model.

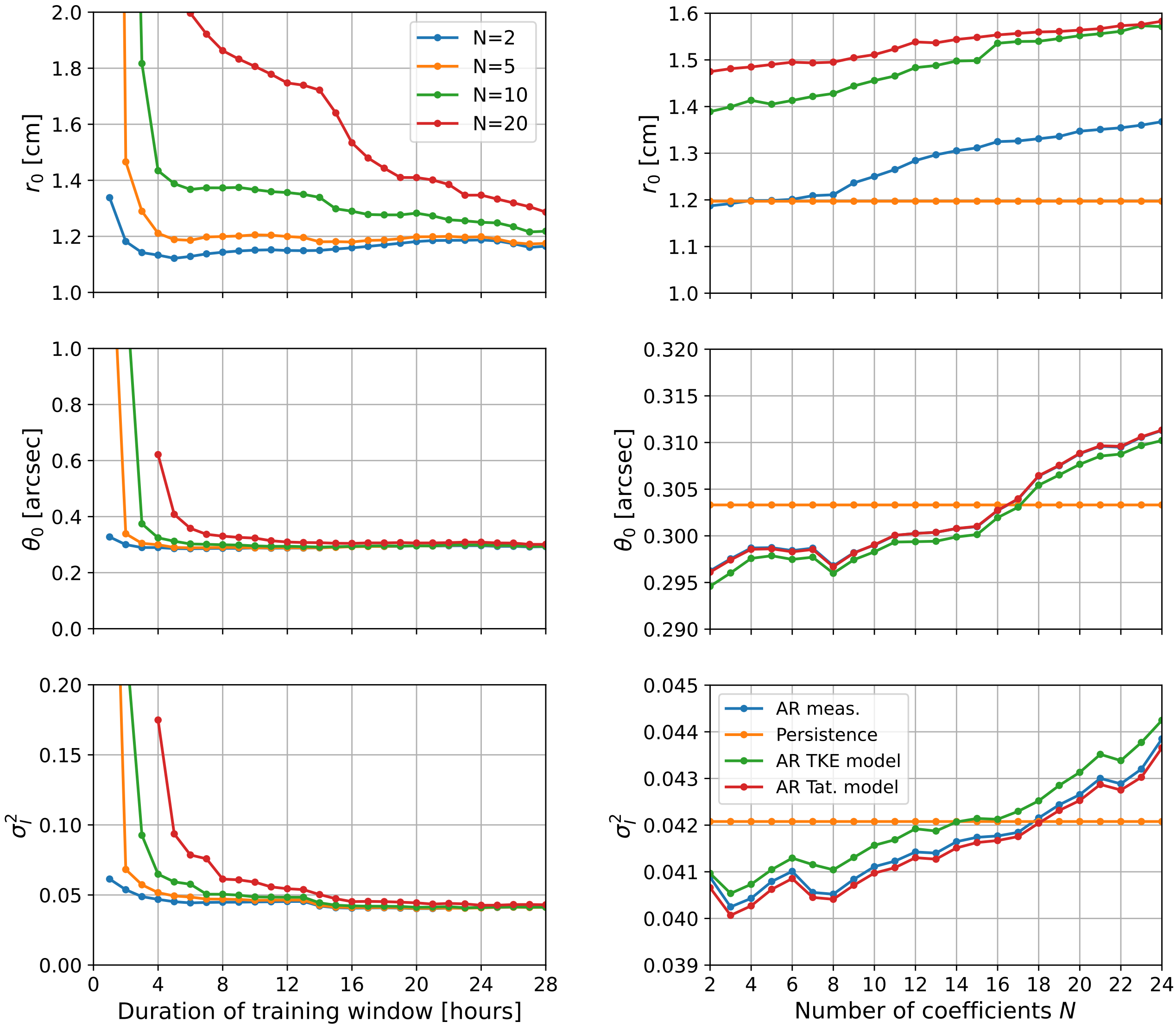

(a) Training window duration.

(b) Number of coefficients.

Figure 3: Evolution of RMSE on the integrated parameters by varying the training window duration and the number of coefficients in the AR models.

4.1 Training window duration

Figure 3a shows the relationship between the root-mean-square error (RMSE), defined below in (5), and the training window duration for different AR models with varying numbers of coefficients ($N = 2, 5, 10$, and 20). The RMSE is calculated for one-step ahead predictions using the AR model on the measurements in (2) and averaged over the entire 84-hour sliding window process (as depicted in Figure 2). The results indicate that increasing the number of autoregressive coefficients requires a longer training window to reduce prediction errors effectively. However, the RMSE reaches an asymptotic limit, beyond which further increasing the number of coefficients or extending the training window does not significantly reduce the error. The convergence to this limit is faster for the isoplanatic angle and scintillation index compared to the Fried parameter.

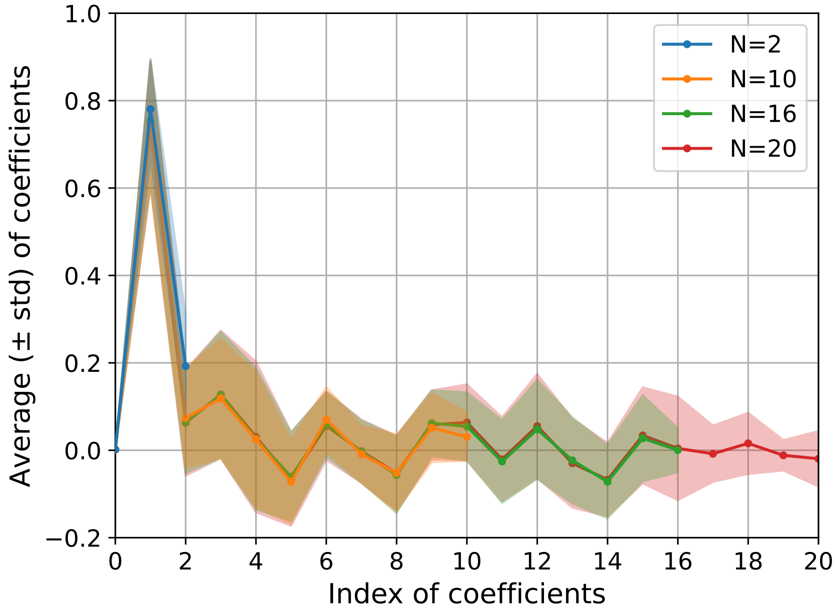

Figure 4: Average ($\pm$ standard deviation) of the AR model coefficients (on Fried parameter).

4.2 Number of coefficients in the autoregression

The evolution of the one-step ahead prediction RMSE is presented in Figure 3b for the different AR models, using a 24-hour training window. The RMSE associated to the persistence model are also depicted, for reference.

Interestingly, as the number of coefficients in the AR models increases, the RMSE tends to rise, indicating a degradation in prediction accuracy. This effect is relatively marginal but more pronounced for the Fried parameter, for which it is partially explained by the limited duration of the training window (observed in Figure 3a). Both AR models based on measurements and NWP modelling errors exhibit similar trends.

Regarding the comparison with the persistence model, it appears that AR models with small numbers of coefficients offer better performance for the one-step ahead prediction of isoplanatic angle and scintillation index. However, this is not the case for the Fried parameter, where the persistence model has the smallest RMSE. The autoregression on the measurements also provides improved short-term forecasts than the autoregressions on the TKE or the Tatarskii+BL modelling errors.

A possible explanation of the small influence of the number of coefficients on the performance metrics can be seen in Figure 4. It depicts the averages and standard deviations of all AR coefficients computed with the sliding training window, for the AR model on the Fried parameter measurements. The coefficient index is given on the x-axis, where the coefficient 0 is the constant α_0 added to the autoregression (fitted close to 0). The dominance of the first coefficient α_1 is clearly visible, and also explains the good performance of the persistence model (i.e., AR model with $\alpha_1 = 1$ and other coefficients equal to zero). The diminishing importance of large coefficients is visible, as their averages get closer to zero. They tend to alternate between opposite positive and negative values, thus partially cancelling each other in the autoregression. Similar behaviours are observed for autoregressions on the isoplanatic angle and the scintillation index.

4.3 Forecast time-horizon

The performance for multistep predictions using AR models with $N = 4$ coefficients and an 8-hour training window is evaluated in Figure 5.

As the prediction window extends from 5 to 60 minutes, RMSE increases for all short-term prediction methods. The short-term approaches consistently outperform NWP long-term forecasts (RMSE shown by the dashed lines),

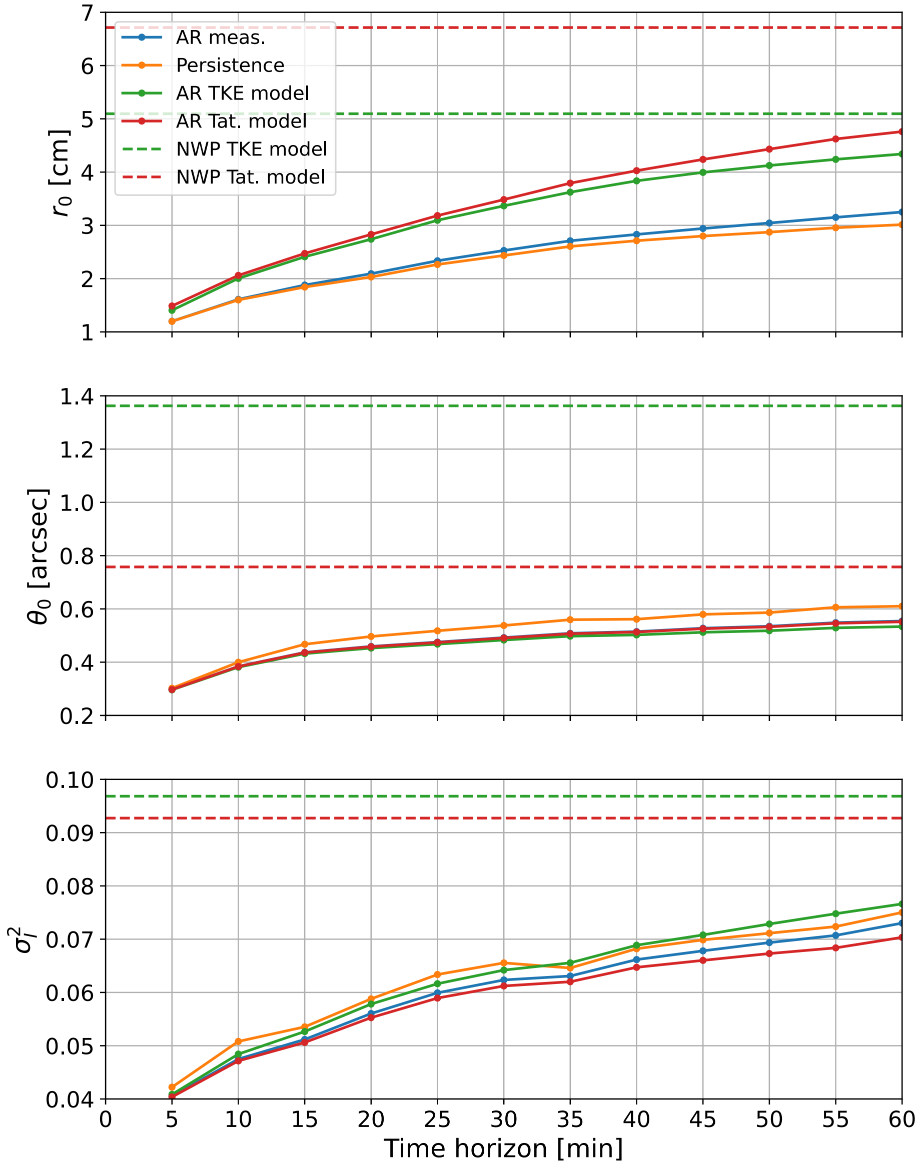

Figure 5: Influence of time-horizon on AR short-term forecasts.

highlighting the benefit of combining NWP forecasts with recent measurements through autoregressions. While AR models generally yield lower RMSE than the persistence model for the isoplanatic angle and scintillation index, the persistence model remains superior for predicting the Fried parameter over short time horizons.

The observations presented in this section are based on a limited dataset and will need further validation as additional data are collected. However, they support the use of AR models with a small number of coefficients, such that short training windows can be used. This is particularly relevant for practical applications where a limited number of measurements may be available before forecasting.

5. APPLICATION AND EVALUATION OF SHORT-TERM FORECAST

This section presents the evaluation of short-term forecast methods applied to the Paranal and Barcelona datasets. For each dataset, the AR models utilize $N = 4$ coefficients (plus a constant), estimated over 4-hour training windows. Performance metrics, including RMSE, mean relative error (MRE), and Pearson correlation coefficient ρ_y, are monitored for the OT integrated parameters and averaged over the entire dataset duration. Both one-step ahead predictions (with a 5-minute time horizon) and multistep ahead predictions (spanning three steps with a 15-minute time horizon) are analysed. The definitions of the RMSE and MRE are

$$\text{RMSE} = \sqrt{\frac{1}{N_\text{obs}} \sum_{i=1}^{N_\text{obs}} \left(\hat{y}_i - y_i\right)^2} \qquad \text{and} \qquad \text{MRE} = \frac{1}{N_\text{obs}} \sum_{i=1}^{N_\text{obs}} \left| \frac{\hat{y}_i - y_i}{y_i} \right|, \tag{5}$$

with N_obs the total number of observations in each dataset when using 4-hour training windows.

Tables 1 to 3, in Appendix A, present the error metrics for the short-term forecasts at Paranal and Barcelona (November 2023 and May 2024). Numbers in parentheses are associated to the multistep ahead predictions (15 minutes), while other numbers correspond to the one-step ahead predictions (5 minutes). Based on their analysis, the following conclusions are drawn:

- **RMSE**: the RMSE values obtained for the integrated parameters, particularly for the Fried parameter, are consistent with those reported in the literature.[10,15] However, it is important to note that different datasets were used in these studies, and that the current analysis includes both nighttime and daytime data.
- **RMSE gains on NWP models**: incorporating recent measurements with an autoregression on the modelling error significantly enhances the performance of both NWP models (TKE and Tatarskii+BL models). The RMSE gain, defined as the ratio of RMSE from NWP-only models (NWP TKE and NWP Tat. models) to that from NWP combined with measurements (AR TKE and AR Tat. models), ranges from 3 to 5.7 for the Fried parameter, depending on the dataset. For the isoplanatic angle, gains vary between 2.6 and 7.3, while for the scintillation index, they range from 1.5 to 4. Similar RMSE gains for seeing are reported in the literature.[9] These RMSE gains are influenced by both the accurate parameterization of AR models and the initial accuracy of the NWP predictions.
- **MRE**: MRE values for the persistence and AR models are between 10 to 20%, depending on the integrated quantity and dataset. This is significantly lower than the MRE observed for NWP models, which can exceed 100%.
- **Correlation coefficients**: maximal values of the correlation coefficients are achieved by the persistence model.
- **Best performance**: considering all metrics, integrated quantities and datasets, the persistence model generally offers the best performance for both 5 and 15-minute predictions. This contrasts slightly with the results observed in Section 4 where AR models sometimes outperform the persistence model. This difference is largely due to the smaller training window used in the current evaluation (4-hour). The AR model on the measurements ranks second in terms of performance.
- **NWP models**: the TKE model provides lower RMSE for the Fried parameter compared to the Tatarskii+BL model. Conversely, the Tatarskii+BL model yields better estimates of θ_0. These conclusions remain valid even after applying AR models, although the differences between the NWP models diminish, particularly for the isoplanatic angle.
- **Time horizon**: as expected, increasing the prediction time horizon reduces the accuracy on the predicted quantities, for all datasets.

Hence, integrating recent measurements with NWP models is essential for significantly improving short-term predictions. However, when such measurements are available, simpler approaches like persistence models or autoregressions on the measurements may provide the best forecasts without the need for long-term predictions. Nevertheless, these conclusions should be further validated due to the limited size of the datasets used. Additionally, the findings depend on the quality of the NWP forecasts, and NWP models that are specifically designed and calibrated for particular locations may enhance long-term forecasts, potentially adding value to short-term predictions.[9]

6. DISCUSSION

The AR models introduced in this work are linear short-term forecast methods that rely exclusively on the time series of the specific OT parameter of interest. Incorporating external inputs, such as meteorological surface measurements, or using non-linear machine learning approaches, as discussed in Section 2, could further enhance their performance.

Furthermore, the parameterization of the AR models was determined through a parameter study conducted solely on Paranal data. Results may vary when using different datasets, recommending further validation. For example, the selection of the number of coefficients N can be made data-dependent.[15] Introducing seasonality into the AR models is another possibility, given that large correlations between measurements separated by 24 hours have been observed in all datasets. Decomposing the time series into various modes for autoregression is another potential approach.[16,19]

Finally, improvements of NWP long-term predictions, specifically for their application to OGS sites, are required,[1] and will benefit both long-term and short-term forecasts.

7. CONCLUSION

The application of AR models for OT short-term forecasting shows significant improvements in the accuracy of NWP model predictions, thanks to the incorporation of on-site measurements. AR models that rely solely on these measurements or simple persistence models also demonstrate strong predictive capabilities.

While the conclusions obtained depend on the AR model parametrization, the datasets used, and the specific NWP models applied, they offer valuable insights into the design of AR models. In particular, they advocate for few coefficients in the autoregressions, allowing for shorter training sequences.

This work highlights the importance of collecting on-site measurements at optical communication sites, for improving long-term predictions from NWP models and for developing short-term forecast approaches.

ACKNOWLEDGMENTS

FQ thanks Guillaume Thiran for valuable discussions contributing to this work. RG acknowledges his Science and Technology Facilities Council studentship 2419794 and funding for the 24hSHIMM development under UK Research and Innovation (MR/S035338/1). The present research is part of the Space4ReLaunch project, which is supported by the SPW Economie Emploi Recherche of the Walloon Region, under the grant agreement No. 2210181.

REFERENCES

[1] Quatresooz, F., Orban de Xivry, G., Absil, O., Vanhoenacker-Janvier, D., and Oestges, C., "Challenges for optical turbulence characterization and prediction at optical communication sites," in [*International Conference on Space Optics—ICSO 2022*], **12777**, 2410–2424, SPIE (2023).

[2] Griffiths, R., Bardou, L., Butterley, T., Osborn, J., Wilson, R., Bustos, E., Tokovinin, A., Le Louarn, M., and Otarola, A., "A comparison of next-generation turbulence profiling instruments at Paranal," *Monthly Notices of the Royal Astronomical Society* , stae434 (2024).

[3] Tokovinin, A., "Measurement of turbulence profile from defocused ring images," *Monthly Notices of the Royal Astronomical Society* **502**(1), 794–808 (2021).

[4] Griffiths, R., Hartley, K., Osborn, J., Farley, O., Wilson, R., Townson, M., Beesley, L., Rodriguez-Gomez, A., Comeron-Tejero, A., and Alaluf, D., "TURBO: an automatic 24-hour turbulence monitoring station in Barcelona," in [*Adaptive Optics Systems IX*], SPIE (2024).

[5] Ziad, A., Giordano, C., Aresta, A., Aristidi, E., Bailet, C., Berto, F., Bertolin, C., Carbillet, M., Cavazzani, S., Ceus, D., et al., "ANAtOLIA: a mobile station for site availability characterization for optical communications links," in [*International Conference on Space Optics—ICSO 2022*], **12777**, 1104–1115, SPIE (2023).

[6] Osborn, J. and Sarazin, M., "Atmospheric turbulence forecasting with a general circulation model for Cerro Paranal," *Monthly Notices of the Royal Astronomical Society* **480**(1), 1278–1299 (2018).

[7] Masciadri, E., Lascaux, F., Turchi, A., and Fini, L., "Optical turbulence forecast: ready for an operational application," *Monthly Notices of the Royal Astronomical Society* **466**(1), 520–539 (2017).

[8] Quatresooz, F., Griffiths, R., Bardou, L., Wilson, R., Osborn, J., Vanhoenacker-Janvier, D., and Oestges, C., "Continuous daytime and nighttime forecast of atmospheric optical turbulence from numerical weather prediction models," *Optics Express* **31**(21), 33850–33872 (2023).

[9] Masciadri, E., Martelloni, G., and Turchi, A., "Filtering techniques to enhance optical turbulence forecast performances at short time-scales," *Monthly Notices of the Royal Astronomical Society* **492**(1), 140–152 (2020).

[10] Milli, J., Gonzalez, R., Fluxa, P., Chacon, A., Navarette, J., Sarazin, M., Pena, E., Carrasco-Davis, R., Solarz, A., Smoker, J., et al., "Nowcasting the turbulence at the Paranal Observatory," *arXiv preprint arXiv:1910.13767* (2019).

[11] Griffiths, R., Osborn, J., Farley, O., Butterley, T., Townson, M. J., and Wilson, R., "Demonstrating 24-hour continuous vertical monitoring of atmospheric optical turbulence," *Opt. Express* **31**, 6730–6740 (2 2023).

[12] Aussem, A., Murtagh, F., and Sarazin, M., "Dynamical recurrent neural networks and pattern recognition methods for time series prediction: application to seeing and temperature forecasting in the context of ESO's VLT Astronomical Weather Station," *Vistas in astronomy* **38**, 357–374 (1994).

[13] Kornilov, M. V., "Forecasting seeing and parameters of long-exposure images by means of ARIMA," *Experimental Astronomy* **41**, 223–242 (2016).

[14] Ni, W.-J., Shen, Q.-L., Zeng, Q.-T., Wang, H.-Q., Cui, X.-Q., and Liu, T., "Data-driven seeing prediction for optics telescope: from statistical modeling, machine learning to deep learning techniques," *Research in Astronomy and Astrophysics* **22**(12), 125003 (2022).

[15] Li, Y., Li, L., Guo, Y., Zhang, H., Fu, S., Gao, C., and Yin, C., "Atmospheric turbulence forecasting using two-stage variational mode decomposition and autoregression towards free-space optical data-transmission link," *Frontiers in Physics* **10**, 970025 (2022).

[16] Klotz, E., *Availability assessment of AO corrected optical links by machine learning*, PhD thesis (2023).

[17] Turchi, A., Martelloni, G., and Masciadri, E., "Evaluation of filtering techniques to increase the reliability of weather forecasts for ground-based telescopes," in [*Adaptive Optics Systems VI*], **10703**, 1477–1486, SPIE (2018).

[18] Masciadri, E., Turchi, A., and Fini, L., "Optical turbulence forecasts at short time-scales using an autoregressive method at the Very Large Telescope," *Monthly Notices of the Royal Astronomical Society* **523**(3), 3487–3502 (2023).

[19] Li, Y., Zhang, H., Li, L., Shi, L., Huang, Y., and Fu, S., "Multistep ahead atmospheric optical turbulence forecasting for free-space optical communication using empirical mode decomposition and LSTM-based sequence-to-sequence learning," *Frontiers in Physics* **11**, 1070762 (2023).

[20] Cherubini, T., Lyman, R., and Businger, S., "Forecasting seeing for the Maunakea observatories with machine learning," *Monthly Notices of the Royal Astronomical Society* **509**(1), 232–245 (2022).

[21] Hou, X., Hu, Y., Du, F., Ashley, M. C., Pei, C., Shang, Z., Ma, B., Wang, E., and Huang, K., "Machine learning-based seeing estimation and prediction using multi-layer meteorological data at Dome A, Antarctica," *Astronomy and Computing* **43**, 100710 (2023).

[22] Box, G. E., Jenkins, G. M., Reinsel, G. C., and Ljung, G. M., [*Time series analysis: forecasting and control (third edition)*], John Wiley & Sons (1994).

[23] Seabold, S. and Perktold, J., "Statsmodels: Econometric and statistical modeling with python," in [*9th Python in Science Conference*], (2010).

[24] Quatresooz, F., Vanhoenacker-Janvier, D., and Oestges, C., "Daytime forecast of optical turbulence for optical communications," in [*Communication and Observation through Atmospheric Turbulence (COAT) workshop*], (2023).

[25] Skamarock, W. C., Klemp, J. B., Dudhia, J., Gill, D. O., Liu, Z., Berner, J., Wang, W., Powers, J. G., Duda, M. G., Barker, D. M., et al., "A description of the advanced research WRF version 4," *NCAR tech. note ncar/tn-556+ str* **145** (2019).

APPENDIX A. TIME SERIES OF INTEGRATED PARAMETERS AND ERROR METRICS FOR SHORT-TERM FORECASTS

A.1 Paranal campaign

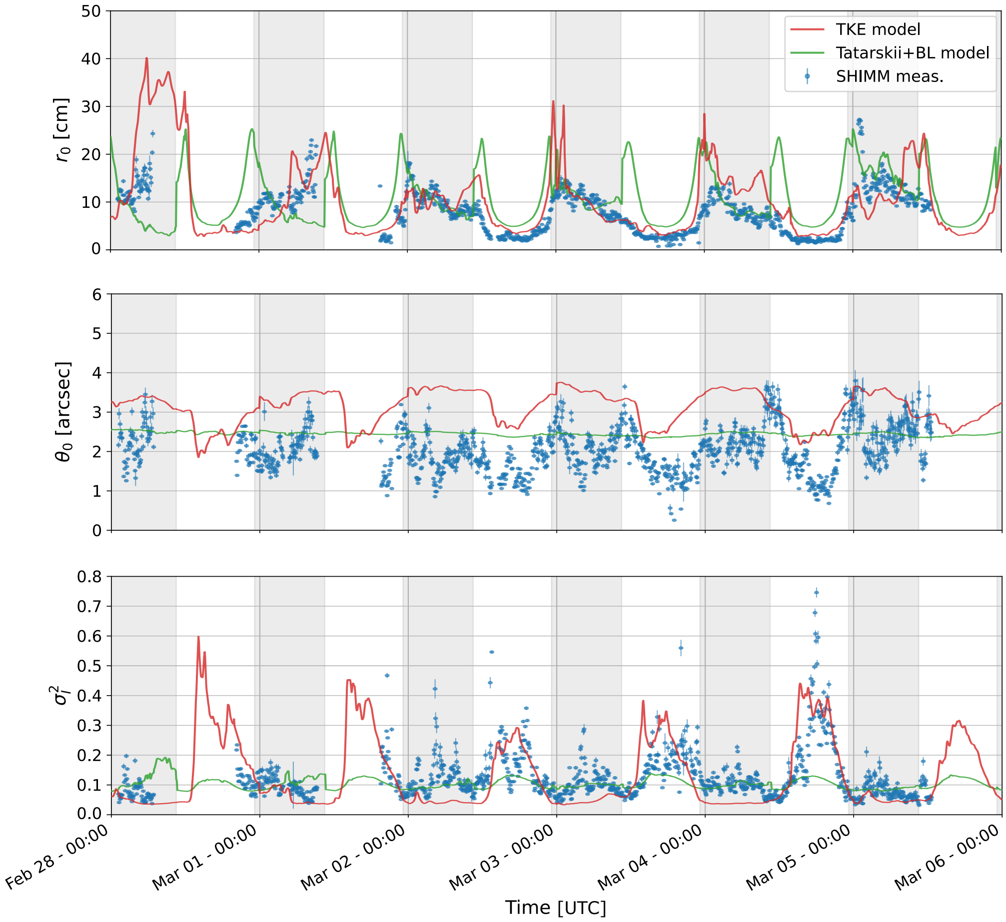

Figure 6: Time series of measured and modelled integrated parameters at Paranal.

Table 1: Error metrics on integrated parameter short-term forecasts for Paranal campaign.

Models	r_0 [cm] RMSE	r_0 [cm] MRE [%]	r_0 [cm] ρ_y	θ_0 [arcsec] RMSE	θ_0 [arcsec] MRE [%]	θ_0 [arcsec] ρ_y	σ_I^2 RMSE	σ_I^2 MRE [%]	σ_I^2 ρ_y
Persistence	1.11 (1.69)	12.21 (17.04)	0.97 (0.93)	0.28 (0.43)	11.71 (17.70)	0.90 (0.76)	0.059 (0.066)	17.78 (27.27)	0.80 (0.75)
AR meas.	1.21 (2.00)	13.19 (18.76)	0.96 (0.91)	0.29 (0.45)	12.59 (18.88)	0.88 (0.72)	0.062 (0.073)	21.12 (31.11)	0.79 (0.74)
AR TKE model	1.47 (2.82)	14.45 (23.83)	0.94 (0.82)	0.29 (0.44)	12.69 (18.95)	0.89 (0.73)	0.061 (0.071)	20.19 (29.97)	0.79 (0.73)
AR Tat. model	1.60 (3.03)	16.61 (30.78)	0.93 (0.80)	0.29 (0.45)	12.60 (18.90)	0.88 (0.72)	0.061 (0.071)	21.08 (30.97)	0.79 (0.74)
NWP TKE model	5.10	61.03	0.60	1.36	77.38	0.38	0.097	49.80	0.56
NWP Tat. model	6.71	110.35	0.46	0.76	43.08	0.23	0.093	34.60	0.47

A.2 Barcelona campaign (November 2023)

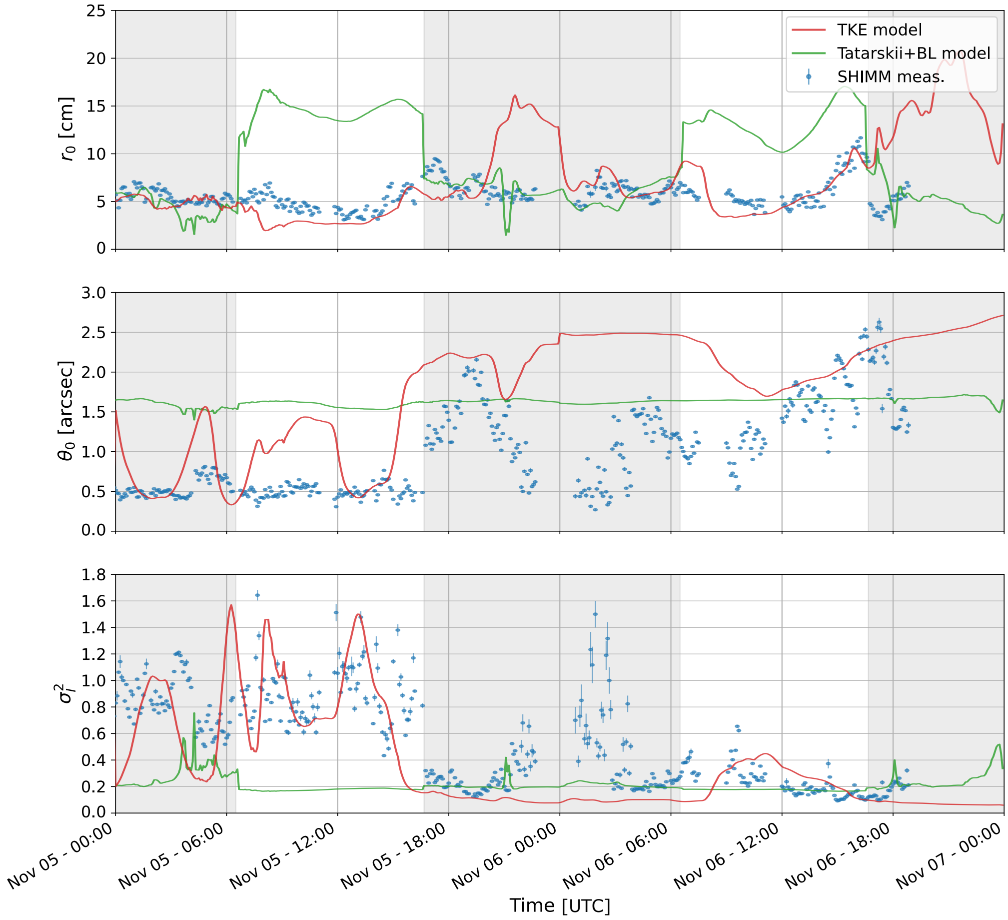

Figure 7: Time series of measured and modelled integrated parameters at Barcelona, in November 2023.

Table 2: Error metrics on integrated parameter short-term forecasts for Barcelona campaign (November 2023).

Models	r_0 [cm] RMSE	r_0 [cm] MRE [%]	r_0 [cm] ρ_y	θ_0 [arcsec] RMSE	θ_0 [arcsec] MRE [%]	θ_0 [arcsec] ρ_y	σ_I^2 RMSE	σ_I^2 MRE [%]	σ_I^2 ρ_y
Persistence	0.64 (0.95)	7.47 (12.09)	0.90 (0.78)	0.16 (0.25)	10.75 (16.96)	0.96 (0.89)	0.144 (0.212)	16.43 (28.02)	0.91 (0.80)
AR meas.	0.68 (1.02)	8.50 (13.23)	0.89 (0.74)	0.18 (0.27)	11.51 (18.36)	0.95 (0.87)	0.156 (0.229)	22.13 (40.21)	0.89 (0.75)
AR TKE model	0.79 (1.49)	10.19 (19.68)	0.85 (0.55)	0.20 (0.30)	12.82 (23.51)	0.93 (0.85)	0.163 (0.266)	22.08 (40.86)	0.88 (0.70)
AR Tat. model	1.08 (2.01)	11.44 (20.38)	0.75 (0.44)	0.19 (0.29)	11.97 (18.99)	0.93 (0.85)	0.160 (0.239)	23.48 (42.20)	0.88 (0.73)
NWP TKE model	3.04	36.45	0.32	0.96	111.53	0.54	0.346	49.13	0.62
NWP Tat. model	6.14	96.77	-0.07	0.84	128.27	0.54	0.470	50.86	0.22

A.3 Barcelona campaign (May 2024)

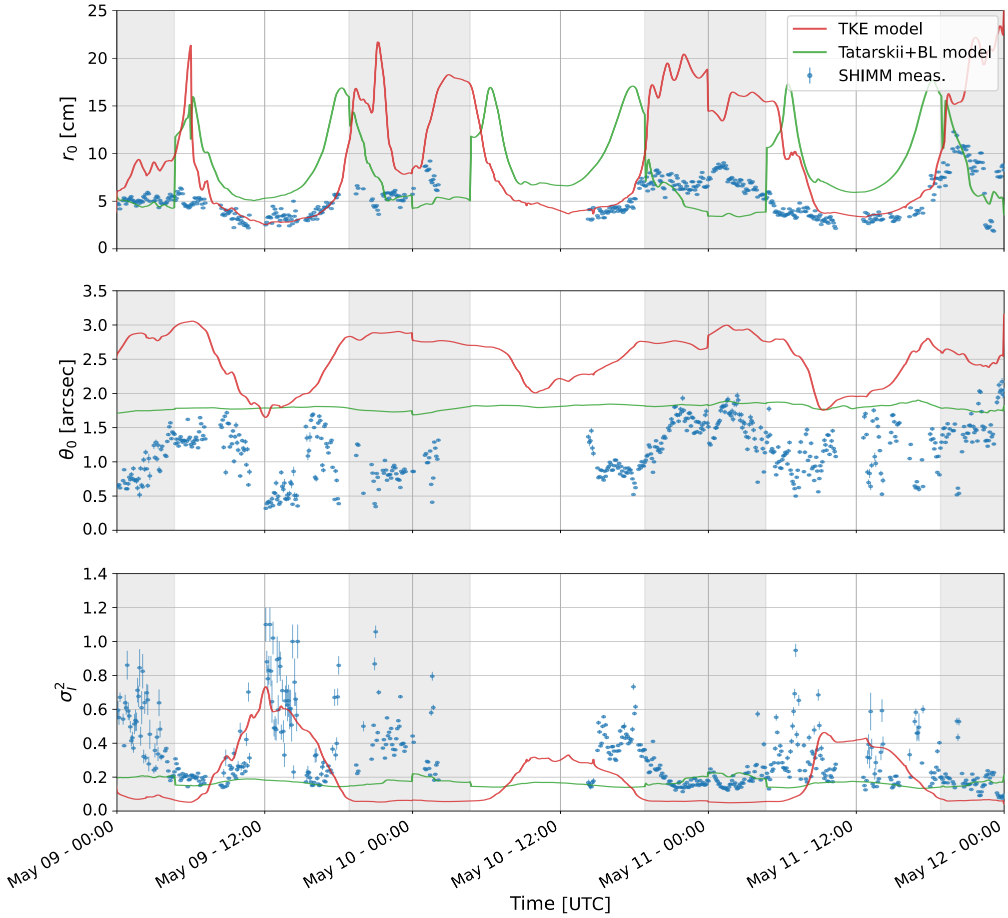

Figure 8: Time series of measured and modelled integrated parameters at Barcelona, in May 2024.

Table 3: Error metrics on integrated parameter short-term forecasts for Barcelona campaign (May 2024).

Models	r_0 [cm] RMSE	r_0 [cm] MRE [%]	r_0 [cm] ρ_y	θ_0 [arcsec] RMSE	θ_0 [arcsec] MRE [%]	θ_0 [arcsec] ρ_y	σ_I^2 RMSE	σ_I^2 MRE [%]	σ_I^2 ρ_y
Persistence	0.58 (0.89)	6.39 (10.11)	0.95 (0.89)	0.18 (0.27)	9.95 (16.76)	0.88 (0.73)	0.112 (0.150)	15.67 (26.06)	0.83 (0.70)
AR meas.	0.62 (0.97)	7.27 (12.00)	0.95 (0.87)	0.19 (0.29)	11.84 (20.12)	0.86 (0.66)	0.117 (0.164)	21.74 (35.91)	0.80 (0.60)
AR TKE model	1.17 (3.67)	11.19 (27.17)	0.85 (0.47)	0.20 (0.31)	12.54 (22.04)	0.84 (0.63)	0.119 (0.189)	22.09 (37.12)	0.79 (0.52)
AR Tat. model	1.71 (2.03)	12.41 (22.82)	0.72 (0.56)	0.20 (0.30)	11.94 (20.44)	0.84 (0.64)	0.117 (0.169)	22.00 (36.97)	0.80 (0.60)
NWP TKE model	6.57	87.89	0.56	1.45	152.33	0.14	0.264	65.75	0.18
NWP Tat. model	5.12	88.04	-0.01	0.75	82.55	0.23	0.244	37.13	-0.01